Advances in Computational Design, *Vol. 11, No. 1 (2026) 17-32*
https://doi.org/10.12989/acd.2026.11.1.017

Techno-Press

Enhanced detection of leiomyosarcoma using opsit and LSTM-GRNN for improved medical image analysis

G. Petchinathan[1], Parveen Begam Abdul Kareem[2], Shanmugaraja P.*[3], Anita Venaik[4] and Selva Lakshmi C.B.[5]

[1]*Department of Biomedical Engineering, Sri Shanmugha College of Engineering and Technology, Pullipalayam, Morur, Sankari (Tk), Salem (Dt.)*
[2]*Department of Computer Science and Engineering, Taibah University, Yanbu, Saudi Arabia*
[3]*Department of InformationTechnology, Sona College of Technology, Salem, Tamil Nadu India*
[4]*Department of InformationTechnology, Amity Business School, Amity University, Noida, India*
[5]*Department Computer Science and Engineering, Velammal College of Engineering and Technology, Madurai, Tamil Nadu, India*

(Received July 29, 2025, Revised October 19, 2025, Accepted October 20, 2025)

Abstract. Leiomyosarcoma is a rare type of cancer that spreads to various parts of the body to create an aggressive form of complex tissue sarcoma disease. Artificial Intelligence (AI) powered technologies play a vital role in screening medical images to identify sarcoma types of diseases for early diagnosis and treatment to avoid cancer risks. In the preliminary stages, the machine learning and deep learning models potentially impact the identification of cancer levels; due to the invasive point of image degradation and feature inconsistency levels, the precision level attains low accuracy, leading to higher false negatives. To solve these problems, to propose an Optimal Particle Swarm Intelligence Technique (OPSIT) for feature selection with Long Short-Term Memory Gated Recurrent Neural Network (LSTM-GRNN) to identify the disease effectively. Initially, a bilateral wavelet filter (BWM) is carried out preprocessing to normalize the feature scaling and improve the image scalar margins. Then, the Linear Reiterative Clustering (LRC) algorithm is applied to segment the non-invasive point of the disease scalar region to split the cancer cells. Further, to scale, the active disease margins in cancer cell features are evaluated with OPSIT to reduce the non-relation feature in the segmented image region. Finally, the LSTM-GRNN algorithm is applied to train the scaled entity of the cancer image region, with Actual threshold margins to identify the disease region accurately. The proposed system increases the proper positive actual scaling region of the cancer region to increase precision rate and attain high accuracy, sensitivity, specificity, and ROC performance compared to the other systems.

Keywords: Bilateral Wavelet Filter (BWM); classification; feature selection; image preprocessing; image segmentation; leiomyosarcoma; Linear Reiterative Clustering (LRC); Long Short-Term Memory Gated Recurrent Neural Network (LSTM-GRNN); Optimal Particle Swarm Intelligence Technique (OPSIT)

1. Introduction

A soft tissue sarcoma is an uncommon kind of tumor that can appear in different body areas; it accounts for less than 1% of all malignancies, with leiomyosarcomas making up approximately

*Corresponding author, Associate Professor, E-mail: shanmugarajap@gmail.com

ISSN: 2092-7614 (Print), 2092-7622 (Online)

25% of newly diagnosed cases. Intraabdominal and retroperitoneal leiomyosarcomas are exceptionally uncommon and have a higher morbidity and mortality rate. Depending on the site of the tumor, leiomyosarcoma of the abdomen and retroperitoneum can manifest with a variety of symptoms. A specific protein, smooth muscle cell actin, can differentiate leiomyosarcoma from other soft tissue sarcomas [1].

Pazopanib, trabectedin, and other chemotherapeutic medications will be used to treat LMS in the future. Immunotherapy has significantly progressed in treating various cancers over the past few decades. Biology of tumors Vaccination has significantly progressed in treating various cancers over the past few periods. Gemstones and docetaxel plus doxorubicin did not significantly differ in median Progression Free Survival (PFS) (5.5 vs. 5.3 months) or Overall Survival (OS) (14.5 vs. 16.3 period). However, the Objective Response Rates (ORR) remained parallel (20 % against 19 %). As an early-line treatment for LMS, doxorubicin and dacarbazine are combined [2].

Increases and decreases of specific chromosomes are among the many chromosomal abnormalities commonly observed in LMS. Chromosomes 1, 10, and 13 may have notable changes. PIK3CA Mutations in the PI3K/AKT pathway can also affect how tumors progress. Alterations in the retinoblastoma protein pathway could cause unchecked cell proliferation. DNA methylation and histone modifications are two examples of molecular classification that can change tumor behavior and impact gene expression in LMS [3].

A specialized sarcoma pathologist must perform a pretreatment sample and subsequent histologic evaluation. Because tumor grades significantly impact prognosis, they should be assigned to every specimen. Data from the National Cancer Database (NCDB) indicates that centralizing treatment for affected roles with Retroperitoneal Sarcomas (RPS) at high-measurement hospitals is associated with better outcomes. Histone and DNA methylation are two epigenetic alterations that can impact tumor behavior and gene expression in LMS [4].

Demographic information, tumor characteristics, surgical techniques, adjuvant treatments, and follow-up results were all collected. Statistical analyses were conducted to assess the factors influencing survival and recurrence. In 22 (29%) of the patients with short-term follow-up (≤2 years), metastases were found in various locations, including 17 lung nodes, three lymph nodes, one renal vein, one liver, and two bones. On Magnetic Resonance Imaging (MRI), neurovascular structures are often associated with lesions that appear isointense (T1), hypointense (T2), or hyperintense (T2 with fat suppression). Depending on their aggressiveness, these lesions may exhibit central bleeding or appear inhomogeneous due to necrosis. The presence of these lesions may be well-defined or may affect the surrounding tissue [5].

The LSTM architecture, a Recurrent Neural Network (RNN), is calculated for regression and classification tasks, particularly with time series data. The second cluster identifies a narrow border of tumor pixels, while Cluster 1 includes non-tumor and tumor regions. When only the vectorized ROI is used (without any transformation), it is found that the third cluster represents the area of interest (ROI/tumor), accurately categorizing 65% of tumor grades. Unlike Long-Term Memory, represented by gradually shifting weights, these feedback connections store activations or representations of recent input occurrences [6].

LSTM-GRNNs can effectively handle complex patterns in data sequences by combining the strengths of LSTM's memory cells with additional gating mechanisms. These mechanisms, including forgetting, input, and output gates, manage information flow and address the issue of vanishing gradients. GRNNs are Recurrent Neural Networks (RNNs) that excel in identifying temporal correlations in sequential input. In binary classification situations, where the dependent variable has two possible outcomes, logistic regression is a commonly used statistical method.

Data transformation can be employed to simplify the categorization process by substituting the label "attack" for non-"normal" outcomes in the "outcome" column [7].

In [8], the Reuters-21578 dataset was used to evaluate the effectiveness of the (Ringed et al.) The RSS-LSTM method aims to balance exploration and exploitation. The performance of deep learning models is heavily influenced by hyperparameters, making it crucial to select the correct settings. This work examines the effectiveness of various metaheuristic methods, specifically Particle Swarm Optimization (PSO), in optimizing hyperparameters in LSTM models. The results demonstrate that metaheuristic-guided optimization improves output metrics and provides valuable insights for ecological monitoring and animal conservation initiatives.

1.1 Contribution of the work

The contribution of the work is the severity classification of leiomyosarcoma cancer detection using a combination of LSTM-GRNN neural networks. This work includes image preprocessing techniques using Bilateral Wavelet Filter (BWM) to reduce distortions and image scalar margins in the input image data. Object detection and clustering are improved through Linear Reiterative Clustering (LRC), which allows for specific cell identification of specific parts without affecting the entire cancer image. The work was done in a cluster using particle swarm optimization (PSO) with the optimized method for particle swarm intelligence (OPSIT) to enhance the feature selection from the images further. Finally, LSTM-GRNN image classification detects the severity of cancer using parameter metrics and memory retention with time series prediction for sequential data.

1.2 Objective

Use a bilateral wavelet filter (BWM) and an image preprocessing technique to improve the unclear area and smooth the image.

To separate internal and outer line regions for finding complex layers using Linear Reiterative Clustering (LRC) image segmentation.

To detect suspicious tissues using Feature Selection using the Optimal Particle Swarm Intelligence Technique (OPSIT).

To identify between regular and typical mammogram severity of leiomyosarcoma cancer using the LSTM-GRNN classification.

2. Literature survey

In [9], Leiomyosarcoma was classified using Doppler ultrasonography using the Toshiba Aplio 500. A linear array transducer operating at 7.5 MHZ was then used to examine the typical femoral vein. A curvilinear transducer operating at 3.5 MHZ was used to observe the external iliac vein. GE Healthcare made the multidetector CT scanner used for CECT. Cancers with vascular origins must be detected early using color Doppler and pulsed-wave Doppler.

A better prognosis for malignant primary cardiac tumors depends on rapid detection and timely treatment. Early detection and treatment are essential for improving patient outcomes in this challenging and frequently misdiagnosed illness. Assessing clinical appearance during the initial evaluation requires examining specific complaints based on their location and severity. These

outputs underline the importance of considering leiomyosarcoma as a potential differential diagnosis for cardiac masses, particularly in cases with unusual clinical symptoms [10].

The limitations of imaging are that while imaging methods such as CT or MRI can detect adrenal masses, accurately distinguish between benign and malignant lesions, and determine the specific type of tumor can be challenging. SMA (Smooth et al.) identification of adrenal masses is even more difficult because many illnesses share similar symptoms, such as weight loss, hormone abnormalities, and stomach pain. Histopathological Difficulties are definitive diagnoses that often require histological investigation, which can be challenging owing to the unusual appearance of the tumor and the need for specific staining methods to confirm smooth muscle distinction [11].

A ULMS database was developed using Artificial Intelligence to identify mitosis. The dataset was obtained from a nearby healthcare center and analyzed by expert professionals. Standard operating procedures were followed for the preprocessing and annotation of the data, and a deep learning-based technique was used to establish baseline accuracies. These modules are made up of the convolution, batch normalization, and leaky-ReLU activation function, as well as the convolution layer and batch normalization layer. This study's output revealed an accuracy of 0.7462, recall of 0.8981, and F1-score of 0.8151 [12].

This work included colon, prostate, testicular, cutaneous, and uterine subtypes, with a total of 20 images per subtype. Of the 20 patients, 10 had benign lesions. This included four patients with normal testicular tissues, three with inflammatory lesions that displayed typical structures and various phases of spermatogenesis but disclosed no signs of malignancy, and three with spermicide maturing stop. Each image was converted to grayscale, 22 texture characteristics were calculated and saved in a file, and each case was represented in a row in the target collection [13].

A specific type of multilayer feedforward network that utilizes an error backpropagation algorithm is known as a Backpropagation (BP) neural network. According to previous reports, the BP algorithm is the basis for nearly 90% of neural network algorithms. The proportion of CD34 in the FS-DFSP group was significantly lower (11.5%) than that in the C-DFSP group (5.1%) ($P=0.005$). FS-DFSP cases had an average Ki-67 index of 18.1%, significantly higher than the average of 8.1% in the C-DFSP cases ($P<0.001$). The training samples for the BP neural network models achieved a classification accuracy of 100 %. The accuracy rates of misdiagnosis and classification were 15.9% and 84.1%, respectively [14].

The mask calibration starts the AC fat extraction process on T1-Weighted MRI images, enabling fat suppression. This procedure is crucial because the AC algorithm requires a Region of Interest (ROI) mask application to segment images. During segmentation, the specified mask must be reduced in size to the position between the fatty tissue and the muscle. The fat in T1-weighted MRI images was effectively segmented by AC using the suggested mask initialization method, yielding F1-scores of 0.89, 0.92, 0.86, and 0.88 [15].

Hemorrhagic degeneration, also called red or cavernous degeneration, can arise from coagulative necrosis caused by infarction of the tumor and acute blockage of the blood supply. The use of fat suppression techniques can result in a loss of Signal Intensity (SI) and distinct fat signal intensity on MRI with high T1WI/T2WI-SI contrast when fatty degeneration, which is frequently observed in lip leiomyomas, is contrasted with tumor necrosis (or CTCN) and hyaline necrosis. The well-defined tumors known as non-degenerated leiomyomas are distinguished by the microscopic arrangement of smooth muscle fascicles and the well-vascularized connective tissue that separates them [16].

Microarray data were acquired from the Gene Expression Omnibus Databases (GSEID: GSE64763 and GSE185543). Data preparation and Differential Gene Expression Analysis (DEGs)

were carried out. A subset of the DEGs found to be common in uterine leiomyoma (ULM) were further validated by intersecting them. Basing itself on Bayes' theorem, the Naive Bayes classifier presumes that features—in this case, genes—are independent. Statistical analysis employed the t-test for group comparisons and the one-way ANOVA for multiple comparisons. $P < 0.05$ was set as the significance level. An enrichment analysis was conducted using $\alpha = 0.05$ [17].

Being able to generate a value between 0 and 1, where 0 denotes a low input value, and 1 denotes a high input value, makes the sigmoid activation function a popular choice among various activation functions. Support vector machines, artificial neural networks, and image processing techniques were used to identify five distinct leukocyte types in the peripheral blood automatically. About 31.16 units is the average measurement of malignant tumors; most readings fall between 1.14 and this range. Most readings fall within 1.28 units of the average measurement of benign tumors, approximately 33.75 units, with a standard deviation of 1.28. 5500 samples from each group were used to examine this output based on a substantial amount of data. [18].

Two MRI tests were performed on each patient, yielding 88 scans. 37 scans were acquired at our facility, while 51 were acquired elsewhere. 44 patients with soft tissue sarcomas who were treated with NAC at our hospital. With AUCs of 0.40 (95 percent CI 0.22–0.58) and 0.44 (95 percent CI 0.26–0.62), the ROC analyses, however, were unable to predict the response to NAC. To determine whole-tumor diameters, a total of 1708 radiomics features were gathered from pre- and post-treatment images using ROIs [19].

Visual representations of diseased tissues have shown promise in quickly identifying drug-sensitive mutant subgroups using Deep Convolutional Neural Network (DCNN) models. This study applied a transfer learning method based on a DCNN to identify instances of drug-sensitive mutations in four distinct network designs. However, disparities were noted amongst institutions, with grayscale images resulting in a 7% drop in accuracy (80 percent accuracy, 87 percent sensitivity, and 73 percent specificity). Moreover, the accuracy rate dropped by 6% and 8%, respectively, when utilizing images that contained only nuclei (81 percent accuracy, 87 percent sensitivity, and 73 percent specificity) or cytoplasm (79 percent accuracy, 88 percent sensitivity, and 67 percent specificity). These findings suggest that buffering effects might be present among subcellular structures when interpreting DCNN results [20].

Although it is well recognized that venous involvement occurs in HCC and RCC, it is essential to remember that tumor thrombi in the abdominal veins can also be a symptom of other abdominal cancers. These thrombi present as self-expanding, gradually increasing filling defects in venous structures. Accurate diagnosis of endogenous tumor thrombus in the abdomen is crucial as it can impact the course of medicinal and surgical treatment. One such uncommon tumor is leiomyosarcoma, which appears to be one of the most common primary tumors of the abdominal vasculature [21].

Palpable lumps, pelvic pain, and irregular bleeding are some of the common symptoms of uterine leiomyosarcoma (ULMS). In order to collect morphological data for this study, descriptions of gross pathology were reviewed. They recorded the surgical margins, myometrial invasion pattern, cervical involvement, tumor size, and relationship to the uterine serosa. With a second adjusted risk model that only included the serosal abutment term, there was a strong correlation between disease-specific ($P < 0.8021$ (0.7314–0.8728)) and disease-free ($P < 0.0001$, AUC 0.8268 (0.7619–0.8917)) survival rates. The prognosis for Stage I ULMS is generally better, but recurrence rates are still high [22].

Inter-reader repeatability was evaluated for 16 sarcomas and 26 leiomyomas, while the influence of reader experience was assessed for 29 sarcomas and 30 leiomyomas, using two

Table 1. Details of characteristics types

References	Algorithm used	Limitation and data set	Outcome and gain output
25	Diagnostic Algorithm	Research Electronic Data Capture data set	Sensitivities 83% Specificities 97%
26	Back propagation neural network (BPNN) and Artificial Neural Network (ANN)	Soft Tissue Sarcoma Histopathological,	BPNN 96.36% and ANN 90.91%
27	Convolution Neural Network (CNN)	Machine and Deep Learning Survey	Accuracy 84.3 %
28	General Linear Model (GLM)	Contrast Enhanced Computed Tomography (CECT)	Specificity ranging from 0.78 to 0.97.
29	Diagnostic Algorithms	Soft Tissue Tumors [STTs]	Performance Severity Evaluation
30	Least Absolute Shrinkage and Selection Operator (LASSO) algorithm	Uterine Carcinosarcoma	Multilevel accuracy parameter taken with the mode of operation
31	Convolutional Neural Network (CNN)	Leiomyosarcoma Cancer	Accuracy 79 % Sensitivity 79 % Specificity 78 %
32	Deep Neural Network (DNN)	Sarcoma Identification	Accuracy 92.44 % Sensitivity 92.25 % Specificity 92.55 %
32	Machine Learning Algorithm	uterine sarcoma	Accuracy 91.43 % Sensitivity 88.24 % Specificity 94.44 %

external validation sets. Although the effects of radiation and chemotherapy are still being studied, it is essential to consider each of these risk factors. Malignant Sarcomas of the Uterus: High cellularity is a common characteristic of many tumors, particularly uterine leiomyosarcomas, which can result in limited diffusion. In the training established, 88% (14 out of 16 masses; 95% CI: 64%, 97%) and 100% (26 out of 26 masses; 95% CI: 87%, 100%) were detected and compared to 83% (24 out of 29 masses; 95% CI: 65%, 92%) in the validation collection [23].

Preprocessing and gene selection methods were used to identify transcripts that showed more leiomyosarcoma variation than healthy uterine tissues. Our approach resulted in the selection of 17 genes for the transcriptome-based classification. Additionally, the prediction accuracy of four distinct models, Random Forest (RF), Deep Feedforward Neural Network (DNN), Support Vector Machine (SVM), and Gradient Boosting (GB), was assessed. The data preparation process involved feature selection, data splitting, and within-sample normalization. The DNN classifier showed a sensitivity of 0.88 and 0.77 (8/9 and 7/9) and a specificity of 1.0 (8/8 and 8/8) in two test datasets, indicating an accuracy rate [24].

2.1 Problem statement

The literature performance evaluation discussed above analyzed the identification of leiomyosarcoma cancer severity using metrics such as Accuracy, Specificity, and Sensitivity. Various algorithms, including Backpropagation (BP), Deep Convolutional Neural Network (DCNN), and Deep Feedforward Neural Network (DNN), were used, and their results are shown

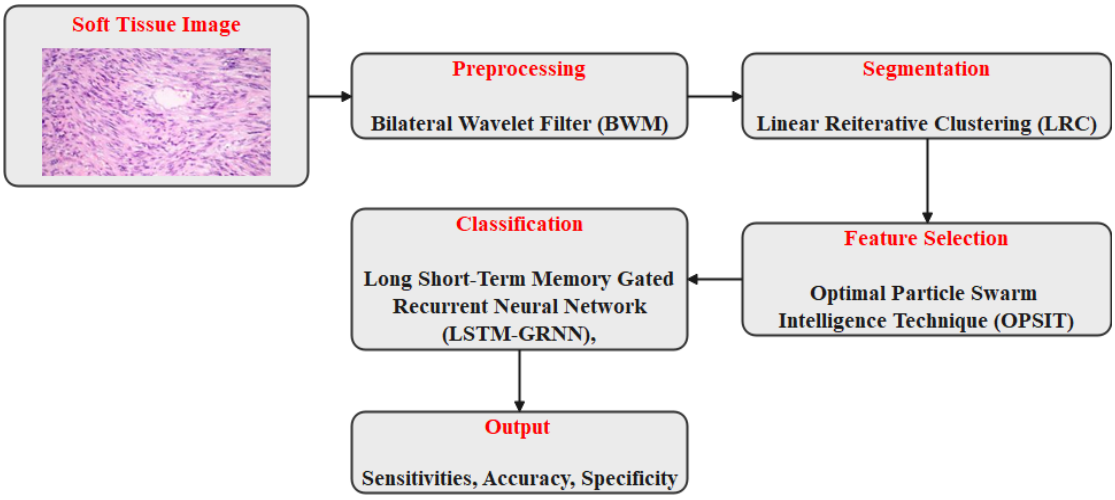

Figure 1. Overall proposed block diagram for leiomyosarcoma cancer

in Table 1. However, Feature extraction methods still require improvement in accurately classifying and segmenting leiomyosarcoma images. The detection of leiomyosarcoma in medical imaging sense modality is by validating image processing techniques.

3. Materials and methodology

Fig. 1 represents the block architecture for the proposed classification method. Initially, Gather Images of Soft Tissue is assembling a group of images depicting soft tissues. Ensure the dataset has a range of samples for trustworthy training and testing. The second Bilateral Wavelet Filter (BWM) reduces noise while preserving edges. Second, clustering segments the preprocessed images using LRC. Start by categorizing the pixels in a preliminary cluster based on their color or intensity. Utilize techniques such as the Histogram of Oriented Gradients (HOG) or Gray Level Co-occurrence Matrix (GLCM) to extract relevant features from the segmented images, such as brightness, texture, and shape. Data preparation involves properly splitting the dataset (e.g., G. to generate the training and testing datasets (80% training, 20% testing), and finally, the LSTM-GRNN model by fusing LSTM layers for sequence learning with GRNN for smooth output. Train the model using the selected attributes from the OPSIT phase to ensure convergence and monitor accuracy and loss during training.

3.1 Preprocessing using bilateral wavelet filter (BWM)

The Bilateral Wavelet Filter (BWM) preprocessing stage operates wavelet analysis to divide the image into distinct frequency components. This helps to scale the input leiomyosarcoma image for feature preservation and reduce noise in targeted regions. In the Selective Filtering stage, a bilateral filter smooths the image while retaining textures through spatial and intensity data. By combining these techniques, the BWM significantly improves image quality for an Adaptive Weighting, particularly in cases where preserving detail is crucial, such as in remote sensing and medical imaging.

$$I\,(x_o, y_0) = \sum_{\alpha=-n} [M(x_o, y_0) - f(x_0, y_0)]^2 \tag{1}$$

In Eq. (1), x_o, y_0 is matrix output layer, (x, y) is non undesirable integrator, Evaluation outcomes demonstrate that the BWM excels in both noise reduction and feature preservation, making it a clear complete image.

$$P^{(K)} = E\left(R_i^{(k+1)}, a, m\right) - E\left(R_i^k, a, m\right) \tag{2}$$

In Eq. (2), Where $P^{(K)}$ makes use of the original seed points, $(k+1)$ is bilateral geographical area technique of progress is the same characterized as pixel-based processing output.

3.2 Segmentation using linear reiterative clustering (LRC)

The Linear Reiterative Clustering (LRC) purposes to improve the sensitivity and specificity of data segmentation in multiple clusters, similar to the Iterative Refinement method. The initialization procedure begins with a preliminary segment deduction, achieved either heuristically or randomly.

$$I_{bw}(x, y) = \int \frac{1\ I_{gray}\,(x, y)\ \geq T}{I_{gray}\,(x, y)\ \geq T} \tag{3}$$

In Eq. (3), where T is the threshold significance, (x, y) is the desired pixel's position, $I_{bw}$is is the binary appearance, and I_{gray} is the grayscale image. The process of extracting features from leiomyosarcoma image data is called feature extraction, including attributes such as color, intensity, appearance, and location.

$$\nabla f(x, y) = \left[\frac{g_x}{g_y}\right] = \left[\frac{\frac{\partial f}{\partial x}}{\frac{\partial f}{\partial x}}\right] \tag{4}$$

In Eq. (4), leiomyosarcoma characteristics help define the gradient of an image, f (x, y), at the location (x, y) of different parts. Distance Calculation uses the extracted features to determine the similarity or distinctiveness of individual pixels or areas. The divided areas of the image are represented by final collections, where each part is a collection of pixels that share similar characteristics.

$$\nabla f \cong |g_x| + |g_y| \tag{5}$$

In Eq. (5), f is a Prewitt range gradation categorization that gets the consequence with the (g_x, g_y) determined filter performance in order to detect boundaries. It carries out convolution by using one-out filtering to determine the gradient. The row and column edge detectors compute the square root of the convolution's amplitude multiplied.

3.3 Optimal particle swarm intelligence technique (opsit) for feature selection

A fitness function is evaluated for each particle, taking into account the features that the particle has chosen. This function classically considers position update or another relevant statistic

and swarm determines the best solution found (global best), while each particle tracks its own best solution (local best). This process continues until a convergence requirement is met or a predetermined number of iterations have been completed. The evolution is optimized based on the specified fitness function, and the threshold represents the improved feature subset discovered during the iterations.

$$\text{Corr}\ (\text{X}_\text{i}\ , \text{Y}) = \frac{\text{cov}\ (\ \text{X}_\text{i}, \text{Y})}{\sigma \text{X}_\text{i}\ \sigma^{\text{Y}}} \tag{6}$$

In Eq. (6) connection between a feature Xi and a target Y may be considered defined mathematically

$$\text{I}\ (X_i, Y) = \sum_{(\text{X},\text{Y})\in \text{R}} [\text{p}(X_i, \text{y}) - \log \frac{\text{p}(X_i, \text{y})}{\text{p}\ (X_i)\ \text{p}(\text{y})}]^1 \tag{7}$$

In Eq. (7) I $(\text{X}_\text{i}, \text{Y})$ describes the selection of features, and more sharing of data evaluations may indicate more significance.

$$C(k, n) = \sum_i \sum_j (i - j)^k\ P_d[i, j]^n \tag{8}$$

In Eq. (8), the measure of local variances in an image is evaluated by the contrast and variance in scores, which increase linearly (0, 1, 2, 3, etc.) as one moves away from the diagonal. This contrasts the exponential increase (0, 1, 4, 9, etc.) seen in Eq. (9) for contrast.

$$\text{D} = \sum_{\text{i,j}=1}^{\text{G}} \text{C}_{\text{i,j}} |\text{i} - \text{j}| \tag{9}$$

3.4 Classification using long short-term memory gated recurrent neural network (LSTM GRNN)

Reducing the complexity of the tissue being processed in the neuron is necessary to produce a smaller network that performs well on test data for classification and training purposes. LSTM of the network type GRNN is used to identify various leiomyosarcoma cancers. Long Short-Term Memory (LSTM) networks are a particular kind of GRNN that was created to solve the problem of disappearing gradients, which are steps used to identify long-term relationships in sequential data. For the current step, the "forget gate" determines which data from the previously hidden state could be remembered and which should be forgotten (Machine Learning Model). According to Machine Learning Models, the input gate controls what information from the current input needs to be included in the subsequent hidden condition. The output of the current step, which is also the next covered state, is determined by the output gate (Medium to high).

$$\text{f}_{(\text{t})} = \sigma\ (\text{W}_\text{f}. |\text{h}_{\text{t}-1}, \text{X}_\text{t}| + \ \text{b}_\text{f} \tag{10}$$

In Eq. (9), The forget gate is activated by f t. For the forget gate, f is the weight matrix. The forget gate's bias is represented by b f. $\sigma\sigma$ is the activation purpose of the sigmoid, and the prior hidden state was ht−1h t−1. There is a current input, x t.

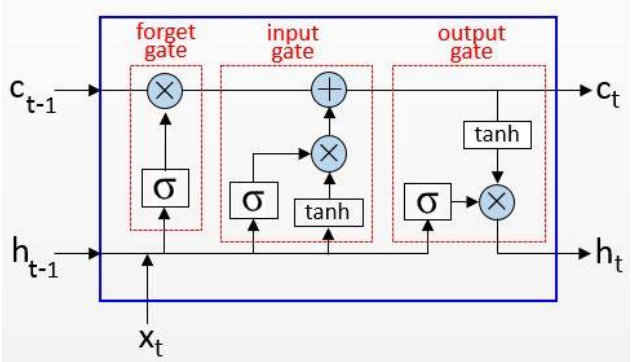

Figure 2. LSTM architecture

3.4.1 LSTM network architecture

The input layer processes sequential information, whereas input patterns are handled by LSTM layers, which can be used in multiples for deeper learning. In Fig. 2, the fully connected (dense) forget gate, which follows the LSTM stages, produces the highest output. Input gate classification task should guide the choice of activation factor. A stochastic activation works better for binary data, but a SoftMax activation is advised for multi-class classification output gate training the model; a loss function is used.

Binary cross-entropy should be used for binary problems; categorical cross-entropy should be used for multi-class problems. An optimizer is employed to minimize the loss operation. Some well-known optimizers are RMSprop and Adam. Backpropagation through time, or BPTT, is used to update the LSTM's weights in response to the loss. Use metrics like accuracy, precision, recall, and F1 score on a validation dataset to assess the model after training. Adjust hyperparameters like batch size, learning rate, number of LSTM layers, and others for better performance.

3.4.2 LSTM GRNN Algorithm

Step 1: Set the parameters to their starting values and assign starting weights to the cell status, inputs, outcomes, and Forget gates.

$$\text{Forget Gate } f_t\text{: } \mathrm{f_t} = \sigma(\mathrm{W_f} \cdot [\mathrm{h_{t-1}}, \mathrm{x_t}] + \mathrm{b_f}) \tag{11}$$

Step 2: The GRNN Model is defined as Constructing an LSTM model that accepts feature vector segments as Input data.

$$\text{Input Gate } \mathrm{i_t}\text{: } \mathrm{i_t} = \sigma(\mathrm{W_i} \cdot [\mathrm{h_{t-1}}, \mathrm{t_x}] + \mathrm{b_i}) \tag{12}$$

Step 3: Utilize a correct loss function while constructing the data structure.

$$\text{Candidate Cell State } \mathrm{C_t}\text{: } \mathrm{C_t} = \tanh(\mathrm{W_c} \cdot [\mathrm{h_{t-1}}, \mathrm{x_t}] + \mathrm{b_C}) \tag{13}$$

Step 4: Implement the provided sequences and matching labels to train the model.

$$\text{Cell State Update } \mathrm{C_t}\text{: } \mathrm{C_t} = f_t\ (\mathrm{C_{t-1}}\ \mathrm{i_t} * \mathrm{X_t}) \tag{14}$$

Step 5: Make predictions by applying the typical functions to predict unique visual quantities.

$$\text{Output gate } o_t\text{: } o_t = \sigma\ (W_o\ .\ [\mathrm{h_{t-1}}, \mathrm{x_t}] + \mathrm{b_0}\ ) \tag{15}$$

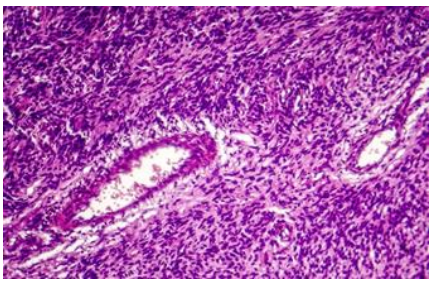

Figure 3. Input soft issue leiomyosarcoma cancer image

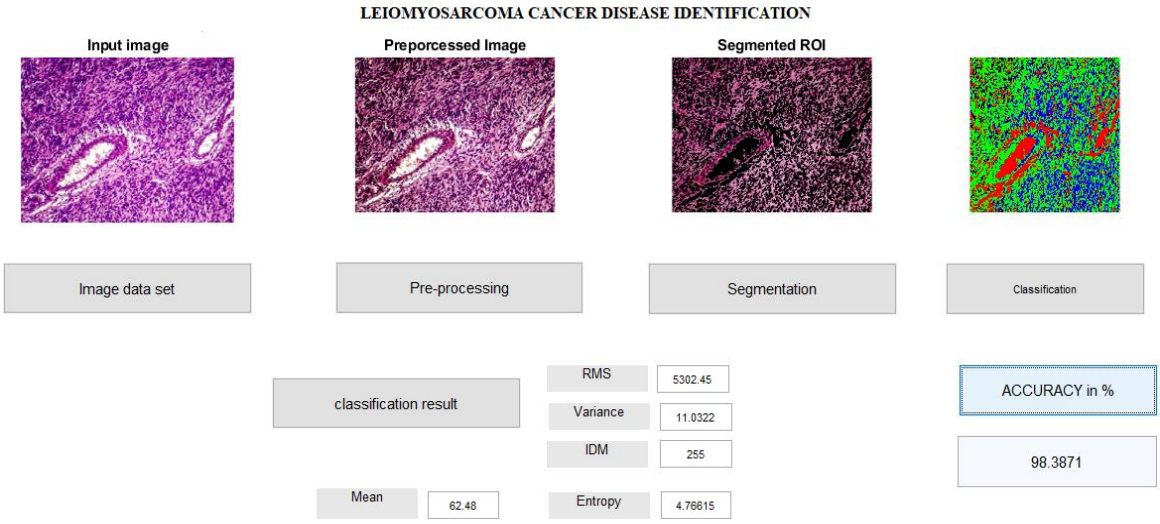

Figure 4. Simulation output of leiomyosarcoma cancer analysis

Step 6: Post-processing includes analyzing the predictions and visualizing the outcomes, such as via ROC curves or confusion matrix structures.

Step 7: Analysis of the variety of leiomyosarcoma cancer, whether regular or abnormal.

Step 8: Based on the classification output, Evaluate the parameters based on accuracy, sensitivity, specificity, and ROC to assess its performance on an evaluation or test set.

4. Experimental output

This experimental result analyzer analyzes the variety of leiomyosarcoma cancer and compares the proposed LSTM-GRNN classification performance with previous research classification techniques.

4.1 Leiomyosarcoma cancer image data set

Fig. 3 shows a dataset of soft tissue cancer images, such as those taken from muscles and skin tissue. This type of cancer, called soft tissue sarcoma, can also affect the lymphatic system, blood vessels, nerves, and structures surrounding joints.

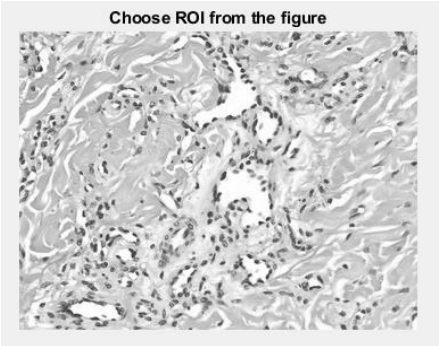

Figure 5. Region of Interest (ROI) output

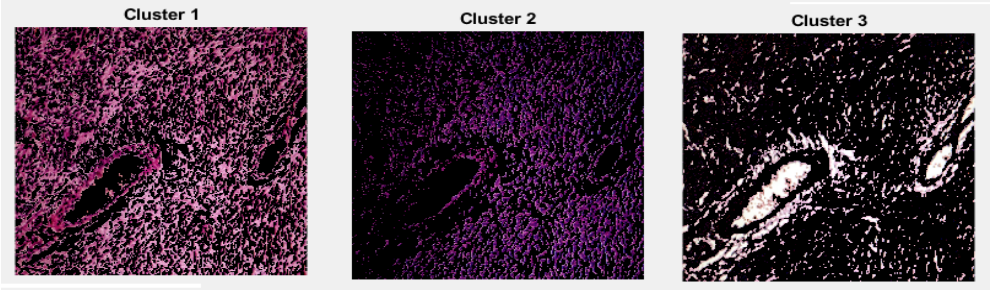

Figure 6. Segmentation clustering output

In Fig. 4, the simulation result has sarcoma cancer data sets and four image processing analyses: image preprocessing, segmentation, feature selection, and classification. This classification technique evaluated the cancer image as either normal or abnormal at the cancer level, and the suggested LSTM-GRNN can more accurately classify the available cancer image.

Fig. 5 shows the output of the ROI sarcoma, which typically includes the ROI coordinates. These coordinates can be represented as bounding box values, such as [x, y, width, height] for rectangles or pixel indices. A binary mask can also be created to label the pixels inside the ROI as 1 (or actual) and the pixels outside as 0 (or false).

Fig. 6 shows how the approach refines clusters in subsequent phases during the iterative clustering process. Linear Reiterative Clustering (LRC) modifies the clustering patterns in each iteration based on the current distribution of the data.

4.2 Classifiers classification measurements

A percentage is frequently used to express accuracy, the degree of precision ascertained by comparing the value to an actual or acceptable value.

$$\text{Accuracy} = 170 + 165 + 1 + 2170 + 165 = 338335 \approx 0.9812 \tag{16}$$

Sensitivity is a real positive rate, another statistic that can be used to calculate the accurate identification rate. A percentage is frequently used to express this,

$$\text{Sensitivity} = 170 + 1170 \approx 0.9642 \tag{17}$$

Table 2. Result of confusion matrix

	Positive	Negative
Positive	True Positive =170	False Positive =1
Negative	False Negative =2	True Negative=165

Figure 7. Comparison analysis of proposed LSTM neural network classification

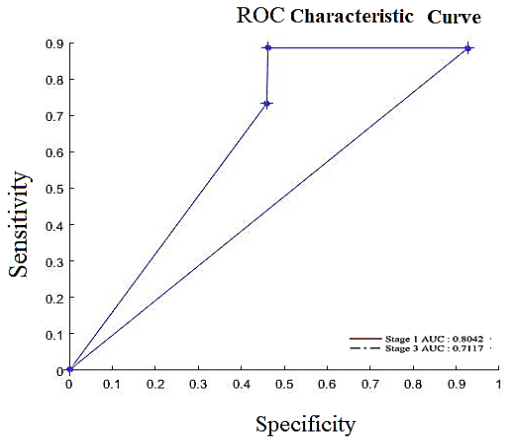

Figure 8. Graph of ROC analysis

Specificity is a performance evaluation statistical metric. Another name for the real negative rate is the actual negative rate, which calculates the percentage of negatively detected parameters. Frequently, this is expressed as a percentage.

$$\text{Recall} = 170 + 2170 \approx 0.9686 \tag{18}$$

The previous research work algorithm used is the Convolutional Neural Network (CNN) [31], with an accuracy of 79%, sensitivity of 79%, and specificity of 78%. The Deep Neural Network (DNN) has an accuracy of 92.44%, sensitivity of 92.55%, and specificity of 92.55%, while the

Machine Learning Algorithm [33] has an accuracy of 91.43%, sensitivity of 88.24% and specificity of 94.44%. The proposed LSTM-GRNN algorithm has a performance level of 96% accuracy, 96% sensitivity, and 98% specificity, as shown in Fig. 7. The analysis of different steps using accuracy, sensitivity, and specificity also supports the high-performance level of the LSTM-GRNN algorithm.

Fig. 8 displays the output of the low error value, which is determined by the true positive and actual negative prediction values calculation of a Receiver operating characteristic curve (ROC).

5. Conclusions

This work the evaluated of a leiomyosarcoma cancer variety classification system and its significance, highlighting that early detection is crucial to enhancing patient care. Bilateral Wavelet Filter (BWM) Increases the efficiency of feature extraction by enhancing image quality during preprocessing. In combination with Linear Reiterative Clustering (LRC), the method accurately identifies relevant features for image segmentation, and ROC is reducing based positive and negative prediction values. In image preprocessing and segmentation, the Optimal Particle Swarm Intelligence Technique (OPSIT) provides a solid basis for enhancing feature selection, particularly for complex medical illustrations such as those about leiomyosarcoma. Finally, employing a confusion matrix, the LSTM-RNN classifies the resulting output of 96% accuracy, 96% sensitivity, and 98% specificity.

5.1 Future Scope

Further, multiple machine-learning approaches are needed to detect various leiomyoma cancer levels. Adding different input cancer image data sets provides more thorough information on sarcomas that may be obtained by combining imaging data with clinical data, electronic healing information, and biomarker information. Moreover, an improved neural network algorithm can be used in real time to manage a sarcoma. Artificial Intelligence can facilitate authentic time clarification of imaging information, qualifying constant monitoring of tumor development and response to treatment.

References

1. Øines, M.N., Smith, H.G., Preisler, L., Penninga, L. (2024). Leiomyosarcoma of the abdomen and retroperitoneum; a systematic review. Frontiers in Surgery, 11, 1375483. https://doi.org/10.3389/fsurg.2024.1375483
2. Lacuna, K., Bose, S., Ingham, M. Schwartz, G. (2023). Therapeutic advances in leiomyosarcoma. Frontiers in Oncology, 13, 1149106. https://doi.org/10.3389/fonc.2023.1149106
3. Kerrison, W.G., Thway, K., Jones, R.L. Huang, P.H. (2023). The biology and treatment of leiomyosarcomas. Critical Reviews in Oncology/Hematology, 184, 103955. https://doi.org/10.1016/j.critrevonc.2023.103955
4. Gamboa, A.C., Gronchi, A., Cardona, K. (2020). Soft-tissue sarcoma in adults: an update on the current state of histiotype-specific management in an era of personalized medicine. CA: A Cancer Journal for Clinicians, 70(3), 200-229. https://doi.org/10.3322/caac.21605
5. Van Beeck, A., Van De Sande, M., Van Praag, V., Dammerer, D., Michielsen, J., Schubert, T., ...

Dijkstra, S. (2020). Clinical outcome of surgically treated leiomyosarcoma of the extremities: a retrospective overview. Anticancer Research, 40(9), 5319-5325. https://doi.org/10.21873/anticanres.14539

6. Fasihi, M.S., Mikhael, W.B. (2021). Brain tumor grade classification using LSTM neural networks with domain pre-transforms. In 2021 IEEE International Midwest Symposium on Circuits and Systems (MWSCAS), 529-532. IEEE. USA, August
7. Purushotam Naidu, K., Deepika, S., Ramya, N.S., Sharmila, N., Vaishnavi, K. Bhavitha, P. (2024). Intrusion Detection System Using Gated Recurrent Neural Network. International Journal of Software Computing and Testing, 10(1), 1-8p.
8. Nasir, M., Samsudin, N.A., Ahmad Khalid, S.K., Baowidan, S., Arshad, H., Sharif, W. (2024). RSS-LSTM: A Metaheuristic-Driven Optimization Approach for Efficient Text Classification. International Journal of Advanced Computer Science & Applications, 15(9). https://doi.org/10.14569/ijacsa.2024.0150929
9. Kim, K., Kim, S., Ahn, T., Kim, H., Shin, S.J., Choi, C.H., ... Suh, D.H. (2023). A differential diagnosis between uterine leiomyoma and leiomyosarcoma using transcriptome analysis. BMC Cancer, 23(1), 1215. https://doi.org/10.1186/s12885-023-11394-0
10. Ayyad, M.S., Elbellasy, M.F., Hassan, A., Gad, M. (2024). Leiomyosarcoma of vascular origin: lessons learned from misdiagnosis. Egyptian Journal of Radiology and Nuclear Medicine, 55(1), 166. https://doi.org/10.1186/s43055-024-01336-6
11. Suzuki, S., Takahashi, N., Sugo, M., Ishiwata, K., Ishida, A., Watanabe, S., ... Yokote, K. (2023). Challenges in the diagnosis of the enigmatic primary adrenal leiomyosarcoma: two case reports and review of the literature. BMC Endocrine Disorders, 23(1), 276. https://doi.org/10.1186/s12902-023-01530-z
12. Zehra, T., Anjum, S., Mahmood, T., Shams, M., Sultan, B.A., Ahmad, Z., ... Ahmed, S. (2022). A novel deep learning-based mitosis recognition approach and dataset for uterine leiomyosarcoma histopathology. Cancers, 14(15), 3785. https://doi.org/10.3390/cancers14153785
13. Atta, I.S., Emam, A.S., Al-Boghdady, A.H., Badran, S.M., El-Refaei, M.F., Abouelatta, O.B. (2022). Assessment of a neural network based on texture features analysis: the impact of classifying cancer types using image processing. American Journal of Biomedical Engineering, 11(1), 1-12. https://doi.org/10.5923/j.ajbe.20221101.01
14. Li, Y., Liang, J., Xu, X., Jiang, X., Wang, C., Chen, S., ... Ji, Y. (2021). Clinicopathological features of fibrosarcomatous dermatofibrosarcoma protuberans and the construction of a back-propagation neural network recognition model. Orphanet Journal of Rare Diseases, 16(1), 48. https://doi.org/10.1186/s13023-021-01698-4
15. Shukor, M.S.M., Meng, B.C.C., Damanhuri, N.S., Othman, N.A., Othman, M.H., Aziz, M.E. (2024). MRI T1 weighted fat segmentation based on active contour for osteosarcoma patients. Journal of Advanced Research in Applied Sciences and Engineering Technology, 49(2), 1-14. https://doi.org/10.36227/techrxiv.175624482.26463371/v1
16. Bura, V., Pintican, R.M., David, R.E., Addley, H.C., Smith, J., Jimenez-Linan, M., Georgiu, C. (2021). MRI findings in-between leiomyoma and leiomyosarcoma: a Rad-Path correlation of degenerated leiomyomas and variants. The British Journal of Radiology, 94(1125), 20210283. https://doi.org/10.1259/bjr.20210283
17. Upadhyay, S., Bhushan, R., Tripathi, A., Chaubey, L., Diwakar, A., Dubey, P.K. (2023). Differential gene expression profile evaluation between uterine leiomyoma and leiomyosarcoma using a machine learning approach. Gynecology and Obstetrics Clinical Medicine, 3(3), 154-162. https://doi.org/10.1016/j.gocm.2023.08.003
18. Atta, I.S., Emam, A.S., Al-Boghdady, A.H., Badran, S.M., El-Refaei, M.F., Abouelatta, O.B. (2022). Assessment of a neural network based on texture features analysis: the impact of classifying cancer types using image processing. American Journal of Biomedical Engineering, 11(1), 1-12. https://doi.org/10.5923/j.ajbe.20221101.01
19. Fields, B.K., Demirjian, N.L., Cen, S.Y., Varghese, B.A., Hwang, D.H., Lei, X., ... Matcuk Jr, G.R.

(2023). Predicting soft tissue sarcoma response to neoadjuvant chemotherapy using an MRI-based delta-radiomics approach. Molecular Imaging and Biology, 25(4), 776-787. https://doi.org/10.1007/s11307-023-01803-y

20. Liang, C.W., Fang, P.W., Huang, H.Y., Lo, C.M. (2021). Deep convolutional neural networks detect tumor genotype from pathological tissue images in gastrointestinal stromal tumors. Cancers, 13(22), 5787. https://doi.org/10.3390/cancers13225787
21. Karaosmanoglu, A.D., Onur, M.R., Uysal, A., Akata, D., Ozmen, M.N., Karcaaltincaba, M. (2020). Tumor in the veins: an abdominal perspective with an emphasis on CT and MR imaging. Insights into Imaging, 11(1), 52. https://doi.org/10.1186/s13244-020-00854-x
22. Chapel, D.B., Sharma, A., Lastra, R.R., Maccio, L., Bragantini, E., Zannoni, G.F., ... Nucci, M.R. (2022). A novel morphology-based risk stratification model for stage I uterine leiomyosarcoma: an analysis of 203 cases. Modern Pathology, 35(6), 794-807.
23. Abdel Wahab, C., Jannot, A.S., Bonaffini, P.A., Bourillon, C., Cornou, C., Lefrère-Belda, M.A., ... Fournier, L.S. (2020). Diagnostic algorithm to differentiate benign atypical leiomyomas from malignant uterine sarcomas with diffusion-weighted MRI. Radiology, 297(2), 361-371. https://doi.org/10.1038/s41379-022-01011-z
24. Afsaneh, E., Sharifdini, A., Ghazzaghi, H., Ghobadi, M.Z. (2022). Recent applications of machine learning and deep learning models in the prediction, diagnosis, and management of diabetes: a comprehensive review. Diabetology & Metabolic Syndrome, 14(1), 196. https://doi.org/10.1186/s13098-022-00969-9
25. Abdel Wahab, C., Jannot, A.S., Bonaffini, P.A., Bourillon, C., Cornou, C., Lefrère-Belda, M.A., ... Fournier, L.S. (2020). Diagnostic algorithm to differentiate benign atypical leiomyomas from malignant uterine sarcomas with diffusion-weighted MRI. Radiology, 297(2), 361-371. https://doi.org/10.1148/radiol.202019165
26. Arunachalam, P., Venkatakrishnan, P., Janakiraman, N. (2021). Histopathology image classification for soft tissue sarcoma in limbs using artificial neural networks. In 2021 6th International Conference on Inventive Computation Technologies (ICICT), 778-785. IEEE. India, January.
27. Madireddy, V., Bommala, H., Yerraboina, S. (2024). Soft tissue sarcoma diagnosis using machine and deep learning-survey. In MATEC Web of Conferences, 392, 01138. EDP Sciences. March.
28. Santoro, M., Zybin, V., Coada, C. A., Mantovani, G., Paolani, G., Di Stanislao, M., ... Perrone, A.M. (2024). Machine learning applied to pre-operative computed-tomography-based radiomic features can accurately differentiate uterine leiomyoma from leiomyosarcoma: A pilot study. Cancers, 16(8), 1570. https://doi.org/10.3390/cancers16081570
29. Crombé, A., Kind, M., Fadli, D., Miceli, M., Linck, P.A., Bianchi, G., ... Spinnato, P. (2023). Soft-tissue sarcoma in adults: Imaging appearances, pitfalls and diagnostic algorithms. Diagnostic and Interventional Imaging, 104(5), 207-220. https://doi.org/10.1016/j.diii.2022.12.001
30. Tsuchihashi, S., Nagawa, K., Shimizu, H., Inoue, K., Okada, Y., Baba, Y., ... Kozawa, E. (2024). Evaluation of uterine carcinosarcoma and uterine endometrial carcinoma using magnetic resonance imaging findings and texture features. Cureus, 16(3). https://doi.org10.7759/cureus.55916
31. Yang, Y., Zhou, Y., Zhou, C., Zhang, X., Ma, X. (2022). MRI-based computer-aided diagnostic model to predict tumor grading and clinical outcomes in patients with soft tissue sarcoma. Journal of Magnetic Resonance Imaging, 56(6), 1733-1745. https://doi.org/10.1002/jmri.28160
32. Toyohara, Y., Sone, K., Noda, K., Yoshida, K., Kato, S., Kaiume, M., ... Osuga, Y. (2023). The automatic diagnosis artificial intelligence system for preoperative magnetic resonance imaging of uterine sarcoma. Journal of Gynecologic Oncology, 35(3), e24. https://doi.org/10.3802/jgo.2024.35.e24